


# Structural changes in Parkinson's disease: voxel-based morphometry and diffusion tensor imaging analyses based on $^{123}\text{I}$ -MIBG uptake

Kazufumi Kikuchi<sup>1</sup> · Akio Hiwatashi<sup>1</sup>  · Osamu Togao<sup>1</sup> · Koji Yamashita<sup>1</sup> · Ryo Somehara<sup>1</sup> · Ryotaro Kamei<sup>1</sup> · Shingo Baba<sup>1</sup> · Hiroo Yamaguchi<sup>2</sup> · Jun-ichi Kira<sup>2</sup> · Hiroshi Honda<sup>1</sup>

Received: 17 February 2017 / Revised: 2 June 2017 / Accepted: 9 June 2017 / Published online: 4 July 2017  
© European Society of Radiology 2017

## Abstract

**Objective** Patients with Parkinson's disease (PD) may exhibit symptoms of sympathetic dysfunction that can be measured using  $^{123}\text{I}$ -metaiodobenzylguanidine (MIBG) myocardial scintigraphy. We investigated the relationship between microstructural brain changes and  $^{123}\text{I}$ -MIBG uptake in patients with PD using voxel-based morphometry (VBM) and diffusion tensor imaging (DTI) analyses.

**Methods** This retrospective study included 24 patients with PD who underwent 3 T magnetic resonance imaging and  $^{123}\text{I}$ -MIBG scintigraphy. They were divided into two groups: 12 MIBG-positive and 12 MIBG-negative cases (10 men and 14 women; age range: 60–81 years, corrected for gender and age). The heart/mediastinum count (H/M) ratio was calculated on anterior planar  $^{123}\text{I}$ -MIBG images obtained 4 h post-injection. VBM and DTI were performed to detect structural differences between these two groups.

**Results** Patients with low H/M ratio had significantly reduced brain volume at the right inferior frontal gyrus (uncorrected  $p < 0.0001$ ,  $K > 90$ ). Patients with low H/M ratios also exhibited significantly lower fractional anisotropy than those with high H/M ratios ( $p < 0.05$ ) at the left anterior thalamic radiation, the left inferior fronto-occipital fasciculus, the left superior longitudinal fasciculus, and the left uncinate fasciculus.

**Conclusions** VBM and DTI may reveal microstructural changes related to the degree of  $^{123}\text{I}$ -MIBG uptake in patients with PD.

## Key Points

- Advanced MRI methods may detect brain damage more precisely.
- Voxel-based morphometry can detect grey matter changes in Parkinson's disease.
- Diffusion tensor imaging can detect white matter changes in Parkinson's disease.

**Keywords** Parkinson's disease · Magnetic resonance imaging · Diffusion tensor imaging · Radionuclide imaging · Neurodegenerative diseases

## Abbreviations

DTI	Diffusion tensor imaging
FA	Fractional anisotropy
H/M	Heart/mediastinum
MD	Mean diffusivity
MIBG	$^{123}\text{I}$ -metaiodobenzylguanidine
MSA	Multiple system atrophy
PD	Parkinson's disease
VBM	Voxel-based morphometry

✉ Akio Hiwatashi  
hiwatashi@radiol.med.kyushu-u.ac.jp

<sup>1</sup> Department of Clinical Radiology, Graduate School of Medical Sciences, Kyushu University, 3-1-1 Maidashi, Higashi-ku Fukuoka 812-8582, Japan

<sup>2</sup> Department of Neurology, Graduate School of Medical Sciences, Kyushu University, 3-1-1 Maidashi, Higashi-ku Fukuoka 812-8582, Japan

## Introduction

Parkinson's disease (PD) is a chronic, progressive, and degenerative neurological disorder, representing the second most frequent neurodegenerative condition, following Alzheimer's disease [1]. PD is clinically characterised by motor symptoms collectively referred to as parkinsonism. The primary

manifestations include resting tremor, slowness when initiating movement, rigidity, and general postural instability [2]. Other non-motor symptoms are also present, such as dysautonomia, cognitive impairment, depression, and olfactory dysfunction [3].

In clinical settings,  $^{123}\text{I}$ -metaiodobenzylguanidine (MIBG) myocardial scintigraphy is used to estimate local myocardial sympathetic nerve damage in a few forms of heart disease [4], autonomic nerve disturbance in diabetic neuropathy [5], and disturbance of the autonomic nervous system in neurodegenerative diseases [6, 7]. Decreased cardiac uptake of  $^{123}\text{I}$ -MIBG has been reported in the early stages of PD, which suggests involvement of the cardiac sympathetic nerve in the early pathogenesis of PD [8]. A recent study revealed that reduced cardiac uptake of  $^{123}\text{I}$ -MIBG suggests cardiac sympathetic denervation and the severity of the accumulation of Lewy bodies. Furthermore, this finding suggested that degeneration of the cardiac sympathetic nerve begins early in the disease process and it occurs before neuronal cell loss in the dorsal vagal nucleus [9].

Conventional magnetic resonance imaging (MRI) usually shows normal features in patients with PD, even in those with long disease duration [10]. Therefore, the essential role of MRI is to exclude secondary causes of the vascular symptoms. Its other role is to assure the absence of specific imaging features found in atypical parkinsonism, such as the hot-cross sign in multiple system atrophy (MSA) [11].

Several advanced MRI techniques can provide quantitative measures of microstructural integrity or morphometric changes in vivo, thus helping detect subtle alterations that are not evident with conventional MRI [10]. A previous study of T2-weighted relaxometry has shown differences in the amount of iron deposits in the basal ganglia between patients and control participants [12]. However, there was a large overlap between the two groups, which limited the conclusions on the diagnostic usefulness of this technique [12]. More recently, voxel-based analysis morphometry (VBM) [13] and diffusion tensor imaging (DTI) [10, 14] have been applied in patients with PD. In VBM analysis, patients with PD showed reduce grey matter volume in the frontal lobe compared to control subjects [13]. In addition, diffusional abnormalities of the frontal white matter have been consistently observed in DTI studies involving patients with PD [15, 16]. Although there are a few previous reports investigating microstructural brain changes between PD patients and healthy controls, only a few reports have revealed the alterations in PD patients with sympathetic dysfunction based on  $^{123}\text{I}$ -MIBG uptake [17]. As stated previously, degeneration of the cardiac sympathetic nerve begins early in the process of PD and that it suggests the severity of the accumulation of Lewy bodies. Therefore, the purpose of this study was to investigate the relationship between microstructural brain changes and  $^{123}\text{I}$ -MIBG uptake in PD patients using VBM and DTI analyses.

## Materials and methods

### Patients

This cross-sectional study was approved by our institutional review boards, and written informed consent was waived. From July 2011 to September 2015, a total of 290 consecutive patients with PD underwent MRI in our institution. All patients were diagnosed with PD by one of two neurologists (H.Y. and J.K.) according to Movement Disorder Society (MDS) clinical diagnostic criteria for PD [18]. Seventeen patients were excluded because they had been finally diagnosed with progressive supranuclear palsy ( $n = 6$ ), MSA ( $n = 4$ ), corticobasal degeneration ( $n = 1$ ), and dementia with Lewy bodies ( $n = 6$ ); 249 patients who previously underwent  $^{123}\text{I}$ -MIBG scintigraphy at another institute or who did not require  $^{123}\text{I}$ -MIBG scintigraphy as per the clinical decision were also excluded. Finally, 24 patients with PD who underwent both MRI and  $^{123}\text{I}$ -MIBG (10 men, 14 women; age range: 60 to 81 years; median age: 67 years) were evaluated. A flow diagram of the study patients is shown in Fig. 1. Disease stage was classified according to the Hoehn and Yahr scale [19] as follows: stage I, six patients; stage II, 10 patients; and stage III, eight patients. Duration of PD from onset ranged from 1 to 6 years (median: 2.2 years). Ten patients exhibited dominant laterality of symptoms on the right side, while 14 patients exhibited that on the left side. All patients underwent evaluation using the Mini-Mental State Examination (MMSE; score range: 23–30, median score: 29). Eleven patients presented with dysautonomia. All patients were treated with levodopa

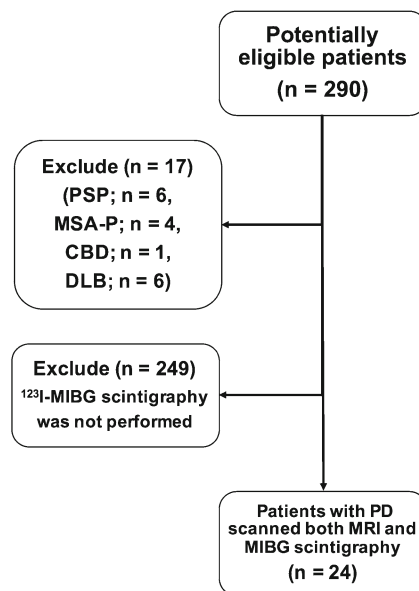


**Fig. 1** Flow diagram of patients. Abbreviations; PSP: progressive supranuclear palsy, MSA-P: multiple system atrophy with predominant parkinsonism, CBD: corticobasal degeneration, DLB: dementia with Lewy bodies

and a dopamine decarboxylase inhibitor at the time of imaging and clinical examination.

## MRI

All MR images were obtained using a 3.0-T system (Achieva; Philips Healthcare, Best, Netherlands) equipped with an eight-channel head coil for sensitivity-encoding parallel imaging. For VBM analysis, high-resolution T1-weighted anatomical images were obtained in the sagittal plane using a magnetisation-prepared rapid gradient-echo sequence (MPRAGE). The sequence parameters were as follows: repetition time (TR), 8.2 ms; echo time (TE), 3.8 ms; inversion time (TI), 1026 ms; flip angle, 8°; field of view (FOV), 240 × 240 mm<sup>2</sup>; acquisition matrix, 240 × 240; slice thickness, 1 mm; number of slices, 190; and acquisition time, 5 min 20 s. For DTI analysis, spin-echo echo planar images were obtained along 15 diffusion gradient directions and with 2 values of b (0 and 800 s/mm<sup>2</sup>). The sequence parameters were as follows: TR/TE, 6000/70 ms; FOV, 230 × 230 mm<sup>2</sup>; matrix, 128 × 96; slice thickness, 2.5 mm; number of slices, 50; and acquisition time, 3 min 51 s.

## <sup>123</sup>I-MIBG scintigraphy

Patients were injected with <sup>123</sup>I-MIBG (111 MBq) intravenously while in the upright position. Single-photon emission computed tomographic (SPECT) images were acquired 15 min after the injection and repeated 4 h later. Anterior and lateral planar images were acquired immediately after each SPECT acquisition. SPECT imaging was performed with a dual-head rotating gamma camera (Infinia Hawkeye, GE Medical Systems, Waukesha, WI, USA) equipped with a low-energy, general-purpose collimator. Images were acquired for 35 s each in 60 steps over a 360° orbit and were recorded at a digital resolution of 64 × 64 pixels. A 20% energy window centred on 159 keV was used. The heart/mediastinum count (H/M) ratio was determined from early and delayed anterior planar <sup>123</sup>I-MIBG images, where H was the mean count/pixel in the left ventricle, and M was the mean count/pixel in the upper mediastinum. The delayed H/M ratio was used as an estimate of cardiac sympathetic activity. The normal value of the H/M ratio in our hospital from healthy volunteers is 2.00 in the late phase. This value was applied for the division of patients into two groups [20].

## Image analysis

### VBM

We evaluated 3D T1-weighted imaging data for group-specific regional atrophy by means of VBM, employing an algorithm called “Diffeomorphic Anatomical Registration

Using Exponentiated Lie Algebra” (DARTEL) [21] implemented in the open source software package SPM12 (<http://www.fil.ion.ucl.ac.uk/spm/>), running in the MATLAB programming environment (R2013a; MathWorks, Natick, MA, USA). Individual images were segmented into grey matter, white matter, and cerebrospinal fluid maps. Next, roughly aligned isotropic (1.0 × 1.0 × 1.0 mm<sup>3</sup>) GM images were obtained such that the images could be imported for subsequent non-linear registration based on an algorithm referred to as DARTEL [21]. A group-specific grey matter template was generated and registered with Montreal Neurological Institute (MNI) standard space. Individual data were co-registered accordingly and smoothed with an 8-mm Gaussian kernel. After global correction for inter-individual total brain volume differences, voxel-wise group statistics were analysed in a whole-brain analysis.

### DTI

DTI was performed with TBSS [21] implemented in FMRIB Software Library 4.1.5 (FSL, Oxford Centre for Functional MRI of the Brain, UK; [www.fmrib.ox.ac.uk/fsl](http://www.fmrib.ox.ac.uk/fsl)). For DTI images, after eddy current correction and brain extraction, fractional anisotropy (FA) maps were computed for all participants. FA data were then analysed via tract-based spatial statistics (TBSS) [22] (FMRIB Image Analysis Group, Oxford, UK [23]) in the following four steps: identification of a common registration target and alignment of FA images of all participants to this target; creation of the mean of all aligned FA images and of a skeletonised mean FA image for the threshold; generation of individual FA skeletons by searching and projecting the maximum FA value along the direction perpendicular to the mean FA skeleton, with the same projections applied to mean diffusivity (MD) for the generation of the corresponding skeletons; and voxel wise statistical analysis of tensor-derived parameters, such as FA and MD, within the skeleton-space. This pipeline was used to analyse both FA and MD images using the FSL tool “randomise”, with 5000 permutations. Any regions on the skeleton showing significant clusters were localised using the “John Hopkins University ICBM-DTI-81 White Matter Labels” and “John Hopkins University White Matter Tractography” atlases in FSL [24].

## Statistical analysis

Patients were divided into two groups according to <sup>123</sup>I-MIBG uptake: high-MIBG uptake and low-MIBG uptake (MIBG<sub>H</sub> and MIBG<sub>L</sub>). We applied a cut-off value of 2.00 for the heart/mediastinum (H/M) ratio calculated using MIBG scintigraphy [20]. The demographic characteristics of the participants are shown in Table 1.

**Table 1** Demographic characteristics of patients

	MIBG <sub>H</sub> (n = 12)	MIBG <sub>L</sub> (n = 12)	p value
Gender, male/female	5/7	5/7	NS
Age (mean, SD)	66.8, 4.9	67.4, 6.1	NS
Hoehn-Yahr stage: 1/2/3	3/7/2	3/3/6	NS
Duration from onset (years)	1, 1.3	2, 1.9	NS
Dominant side of symptom laterality: R/L	7/5	3/9	NS
MMSE	28.5, 1.9	29, 2.4	NS
Presence of dysautonomia	4	7	NS
<sup>123</sup> I-MIBG uptake (H/M ratio)	2.66, 0.4	1.52, 0.2	NA

Abbreviations: MIBG<sub>H</sub>: high MIBG uptake group, MIBG<sub>L</sub>: low MIBG uptake group, NS; not significant, SD; standard deviation, R; right, L; left, MMSE; mini-mental state examination, H/M; heart-to-mediastinum, NA; not applicable

Demographic and clinical variables were compared between groups using the Mann–Whitney U test, or the Chi-square test. Statistical analyses were performed with a commercially available software package (Prism 6.0, GraphPad Software, San Diego, CA, USA). A  $p$  value  $< 0.05$  was considered significant. In VBM analysis, a voxel-by-voxel analysis of covariance (ANCOVA) was computed to detect regional differences in grey matter or white matter volume between the MIBG<sub>H</sub> group and MIBG<sub>L</sub> group using SPM12. The patients' age at the time of MRI, gender, and H/M ratio were entered as the nuisance covariates. An uncorrected  $p$  value  $< 0.0001$  with spatial extent  $K > 90$  voxels was considered significant. In DTI analysis, the randomise option with threshold-free cluster enhancement was applied [25]. All statistical images were corrected for multiple comparisons and thresholded at  $p < 0.05$ .

## Results

With respect to demographic and clinical findings, symptom laterality tended to be frequent on the left side in both groups, while the presence of dysautonomia tended to be frequent among the MIBG<sub>L</sub> group, although there were no statistically significant differences (Table 1).

The differences in grey matter volume between the MIBG<sub>L</sub> and MIBG<sub>H</sub> groups obtained via VBM analysis are depicted in Fig. 2. MIBG<sub>L</sub> patients demonstrated a significant reduction in grey matter volume in the right inferior frontal gyrus (pars opercularis, uncorrected  $p < 0.0001$ ,  $K > 90$ ) compared to MIBG<sub>H</sub> patients. There were no statistically significant differences in grey matter in any other regions of the brain between these two groups.

The differences in FA value observed between the MIBG<sub>L</sub> and MIBG<sub>H</sub> groups in the DTI analysis are shown in Fig. 3. Patients in the MIBG<sub>L</sub> group exhibited significantly lower FA in the left anterior thalamic radiation, the left inferior fronto-occipital fasciculus, the left superior longitudinal fasciculus,

and the left uncinate fasciculus than those in the MIBG<sub>H</sub> group ( $p < 0.05$ ). There were no statistically significant

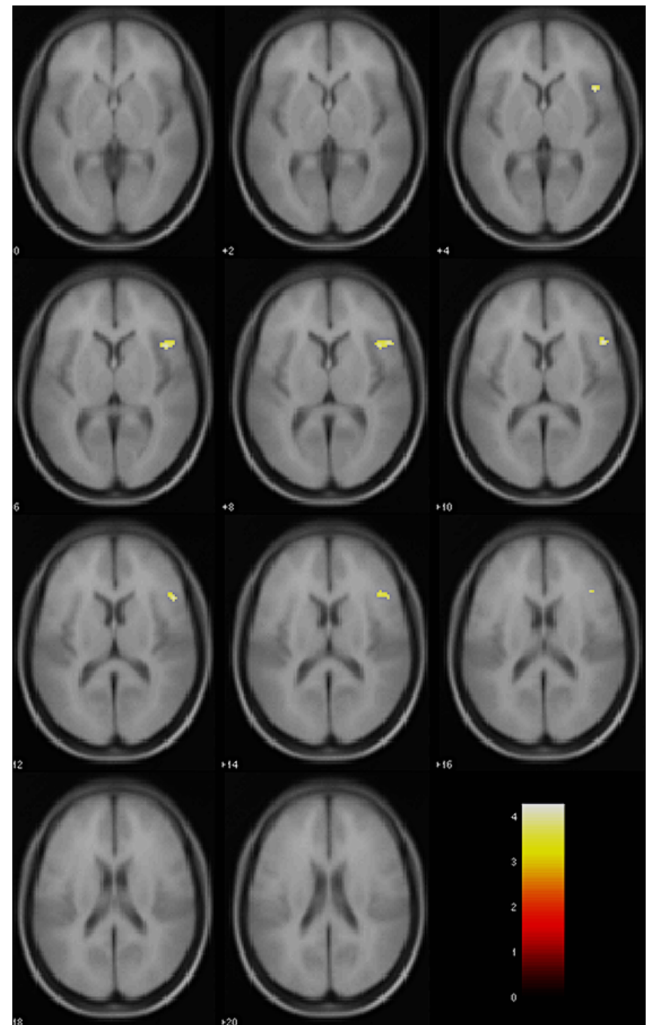


**Fig. 2** Grey matter volume reduction in the MIBG<sub>L</sub> and MIBG<sub>H</sub> groups observed by VBM analysis. Grey matter volume was significantly lower in the MIBG<sub>L</sub> group than in the MIBG<sub>H</sub> group at the inferior frontal gyrus (coordinates:  $x = 51.0$ ,  $y = 19.5$ ,  $z = 10.5$ ; pars opercularis) on the right side (uncorrected  $p < 0.0001$ ,  $K > 90$ )



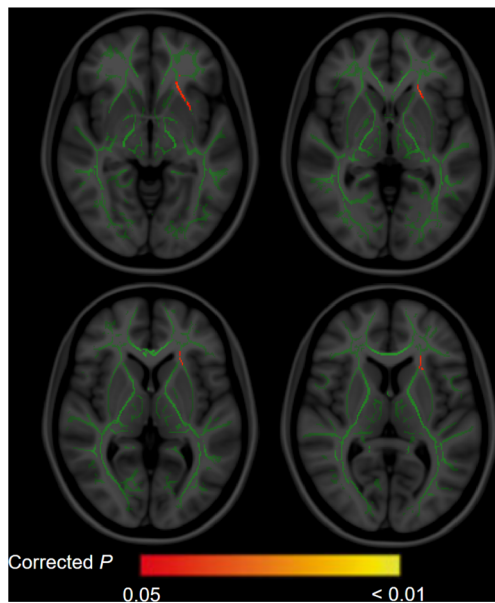


**Fig. 3** FA reduction in the MIBG<sub>L</sub> and MIBG<sub>H</sub> groups observed by DTI analysis. FA value was significantly lower in the MIBG<sub>L</sub> group than in the MIBG<sub>H</sub> group at the anterior thalamic radiation, inferior fronto-occipital fasciculus, superior longitudinal fasciculus, and uncinata fasciculus on the left side ( $p < 0.05$ )

differences in MD in any tracts between the MIBG<sub>L</sub> and MIBG<sub>H</sub> groups ( $p > 0.05$ , data not shown).

## Discussion

In the present study, symptom laterality tended to be frequent on the left side in both groups, while the presence of dysautonomia tended to be frequent among the MIBG<sub>L</sub> group, although there were no statistically significant differences (Table 1). Dysautonomia [26] and motor laterality [27] are well-known aspects of PD. Dysautonomia leads to specific symptoms such as orthostatic hypotension, hypodiaphoresis, urinary dysfunction, and constipation. Dysautonomia is found in the pre-motor early stages of PD and is associated with decreased uptake of <sup>123</sup>I-MIBG [28]. In the present study, we observed that dysautonomia tended to be more frequent among patients with MIBG<sub>L</sub> than among those with MIBG<sub>H</sub>, which is consistent with the findings of previous reports [26, 28]. Motor laterality is a diagnostic clue that can be used to differentiate PD from other motor nerve disorders [27] and is only observed in stage I according to the Hoehn and Yahr scale [19]. As PD progresses, motor laterality decreases.

VBM revealed significant losses in grey matter volume in the right inferior frontal gyrus in the MIBG<sub>L</sub> group. Furthermore, we observed diffuse white matter changes in the anterior thalamic radiation, the inferior fronto-occipital fasciculus, the superior longitudinal fasciculus, and the uncinata fasciculus of the left hemisphere, mainly in the prefrontal

regions, using DTI. Connectivity between the substantia nigra (SN) and prefrontal areas such as the pars opercularis, pars orbitalis, pars triangularis, and rostral middle frontal gyrus has been reported [29]. Similar connectivity has been described in rodents [30], non-human primates [31], and humans by means of DTI-based techniques [29, 32]. Cacciola et al. reported that connections among the pars opercularis, pars orbitalis, and rostral middle frontal gyrus were predominantly right-sided, while other connections were predominantly left-sided, in healthy participants [29]. Our results of VBM suggest that impairment of connectivity between the right SN and inferior frontal gyrus may occur in patients with progressive PD.

Previous region-of-interest diffusion studies of PD have shown reduced FA in specified subcortical structures and cerebral white matter tracts, which is consistent with our results [10, 33]. We have replicated previous findings using whole-brain analysis methods [34], observing reduced FA in the gyrus rectus (olfactory tract), prefrontal white matter, and the corticospinal tract. In the present study, we also identified reductions in FA in the white matter of right prefrontal lobe. Our results suggest that local regions of cerebral white matter are affected in PD patients with sympathetic dysfunction. However, it is difficult to make specific inferences as to the underlying axonal or myelin pathology related to changes in FA and MD using DTI alone [14]. It is well established that a fronto-striatal dysexecutive syndrome or impairment of extrapyramidal system accompanied by grey matter pathology affecting fronto-striatal circuits can be present from the early beginning stages of PD [35, 36]. In the present study, we demonstrated corresponding evidence for fronto-striatal white matter pathology, with reduced FA in right prefrontal white matter tracts and in the external capsules (one of the principal white matter tracts connecting the prefrontal cortex and the striatum). We found that the dominant extrapyramidal symptomatic side corresponded with reductions in FA. Therefore, our results suggest that DTI may detect microstructural changes in the brain of PD patients with sympathetic dysfunction.

According to Braak's model, the accumulation of Lewy bodies occurs during stage V of PD in the grey matter, while stage IV in white matter [37]. This finding must be confirmed via pathological specimen analysis. Our results suggest that advanced MRI techniques including VBM and DTI may be able to detect microstructural changes in PD patients with sympathetic dysfunction, that are related to histopathological accumulation of Lewy bodies in a non-invasive fashion. We further suggest that these advanced MRI methods may be able to detect the areas of brain damage more precisely and potentially lead to improved identification of PD patients with early sympathetic dysfunction, resulting in immediate treatment.

There are a few limitations to our study. First, MRI data were collected as part of a larger PD study in which patients were scanned once while taking dopaminergic medication. However, it is unlikely that the medication contributes to the

differences in diffusion measures for several reasons. The pharmacological action of these drugs is less likely than primary effects of the disease to influence DTI data. A second limitation is that, while the number of participants ( $n = 24$ ) is comparable to several other DTI studies of PD, a few studies used larger numbers of patients to reduce type II error [3, 16, 33, 38]. Our study design was a comparison between PD with MIBG<sub>L</sub> and MIBG<sub>H</sub>, not between PD and healthy control subjects. Our results may differ from healthy controls; however, this study revealed insights into the progression process of PD. The small size of our samples may have limited the comparison of disease severity. PD patients with MIBG<sub>L</sub> are quite rare and it was difficult to conduct a large cohort study. Further multicentre studies are necessary to confirm the conclusions. Furthermore, as the diagnosis of PD was not histopathologically confirmed, the possibility of misdiagnosis remains.

With respect to statistical analysis, there were several options available for determining the significance level. Simply determining statistical significance by a  $p$  value  $< 0.05$  would not account for the multiple comparisons performed within the same subject. However, it has been shown that Bonferroni corrections via family wise error (FWE) are overtly conservative and do not account for the unequal distribution of  $p$  values [39]. The false discovery rate approach (FDR) accounts for this at some level, but still requires the critical threshold for the highest test statistics to depend on a FWE correction, which can lead to a lack or underrepresentation of active voxels [40]. Both corrections were examined in the VBM analysis, resulting in non-significance. However, it was suspected that the issues with FWE and FDR may be at play. A common practice is to report thresholds of uncorrected  $p$  values  $< 0.001$  [40]. We increased this level to uncorrected  $p$  values of  $< 0.0001$ , to avoid the issues observed with FWE and FDR, while being more conservative than common practice.

In summary, cardiac sympathetic denervation represents the severity of the accumulation of Lewy bodies. Our findings indicate that VBM and DTI may reveal microstructural changes related to the degree of MIBG uptake in patients with PD, which, in turn, may indicate the severity of the accumulation of Lewy bodies.

#### Compliance with ethical standards

**Guarantor** The scientific guarantor of this publication is Hiroshi Honda.

**Conflict of interest** The authors of this manuscript declare no relationships with any companies, whose products or services may be related to the subject matter of the article.

**Funding** The authors state that this work has not received any funding.

**Statistics and biometry** No complex statistical methods were necessary for this paper.

**Informed consent** Written informed consent was waived by the institutional review board.

**Ethical approval** Institutional review board approval was obtained.

#### Methodology

- retrospective
- diagnostic or prognostic study
- performed at one institution

#### References

1. de Lau LM, Breteler MM (2006) Epidemiology of Parkinson's disease. *Lancet Neurol* 5:525–535
2. Obeso JA, Rodriguez-Oroz MC, Rodriguez M et al (2000) Pathophysiology of the basal ganglia in Parkinson's disease. *Trends Neurosci* 23:S8–S19
3. Hattori T, Orimo S, Hallett M et al (2014) Relationship and factor structure in multisystem neurodegeneration in Parkinson's disease. *Acta Neurol Scand* 130:347–353
4. Sisson JC, Shapiro B, Meyers L et al (1987) Metaiodobenzylguanidine to map scintigraphically the adrenergic nervous system in man. *J Nucl Med* 28:1625–1636
5. Mantysaari M, Kuikka J, Mustonen J et al (1992) Noninvasive detection of cardiac sympathetic nervous dysfunction in diabetic patients using [123I]metaiodobenzylguanidine. *Diabetes* 41:1069–1075
6. Yoshita M (1998) Differentiation of idiopathic Parkinson's disease from striatonigral degeneration and progressive supranuclear palsy using iodine-123 meta-iodobenzylguanidine myocardial scintigraphy. *J Neurol Sci* 155:60–67
7. Hokusui S, Yasuda T, Yanagi T et al (1994) A radiological analysis of heart sympathetic functions with meta-[123I]iodobenzylguanidine in neurological patients with autonomic failure. *J Auton Nerv Syst* 49: 81–84
8. Orimo S, Takahashi A, Uchihara T et al (2007) Degeneration of cardiac sympathetic nerve begins in the early disease process of Parkinson's disease. *Brain Pathol* 17:24–30
9. Orimo S, Kanazawa T, Nakamura A et al (2007) Degeneration of cardiac sympathetic nerve can occur in multiple system atrophy. *Acta Neuropathol* 113:81–86
10. Gattellaro G, Minati L, Grisoli M et al (2009) White matter involvement in idiopathic Parkinson disease: a diffusion tensor imaging study. *AJNR Am J Neuroradiol* 30:1222–1226
11. Schrag A, Good CD, Miszkil K et al (2000) Differentiation of atypical parkinsonian syndromes with routine MRI. *Neurology* 54:697–702
12. Vymazal J, Righini A, Brooks RA et al (1999) T1 and T2 in the brain of healthy subjects, patients with Parkinson disease, and patients with multiple system atrophy: relation to iron content. *Radiology* 211:489–495
13. Burton EJ, McKeith IG, Burn DJ, Williams ED, O'Brien JT (2004) Cerebral atrophy in Parkinson's disease with and without dementia: a comparison with Alzheimer's disease, dementia with Lewy bodies and controls. *Brain* 127:791–800
14. Rae CL, Correia MM, Alena E, Hughes LE, Barker RA, Rowe JB (2012) White matter pathology in Parkinson's disease: the effect of imaging protocol differences and relevance to executive function. *Neuroimage* 62:1675–1684

15. Karagulle Kendi AT, Lehericy S, Luciana M, Ugurbil K, Tuite P (2008) Altered diffusion in the frontal lobe in Parkinson disease. *AJNR Am J Neuroradiol* 29:501–505
16. Zhang K, Yu C, Zhang Y et al (2011) Voxel-based analysis of diffusion tensor indices in the brain in patients with Parkinson's disease. *Eur J Radiol* 77:269–273
17. Salsone M, Cerasa A, Arabia G et al (2014) Reduced thalamic volume in Parkinson disease with REM sleep behavior disorder: volumetric study. *Parkinsonism Relat Disord* 20:1004–1008
18. Postuma RB, Berg D, Stern M et al (2015) MDS clinical diagnostic criteria for Parkinson's disease. *Mov Disord* 30:1591–1601
19. Webster DD (1968) Critical analysis of the disability in Parkinson's disease. *Mod Treat* 5:257–282
20. Yonezawa M, Nagao M, Abe K et al (2013) Relationship between impaired cardiac sympathetic activity and spatial dyssynchrony in patients with non-ischemic heart failure: assessment by MIBG scintigraphy and tagged MRI. *J Nucl Cardiol* 20:600–608
21. Ashburner J (2007) A fast diffeomorphic image registration algorithm. *Neuroimage* 38:95–113
22. Smith SM, Jenkinson M, Johansen-Berg H et al (2006) Tract-based spatial statistics: voxelwise analysis of multi-subject diffusion data. *Neuroimage* 31:1487–1505
23. Smith SM, Jenkinson M, Woolrich MW et al (2004) Advances in functional and structural MR image analysis and implementation as FSL. *Neuroimage* 23:S208–S219
24. Mori S, Oishi K, Jiang H et al (2008) Stereotaxic white matter atlas based on diffusion tensor imaging in an ICBM template. *Neuroimage* 40:570–582
25. Smith SM, Nichols TE (2009) Threshold-free cluster enhancement: addressing problems of smoothing, threshold dependence and localisation in cluster inference. *Neuroimage* 44:83–98
26. Palma JA, Kaufmann H (2014) Autonomic disorders predicting Parkinson's disease. *Parkinsonism Relat Disord* 20:S94–S98
27. Cubo E, Martin PM, Martin-Gonzalez JA, Rodriguez-Blazquez C, Kulisevsky J, Members EG (2010) Motor laterality asymmetry and nonmotor symptoms in Parkinson's disease. *Mov Disord* 25:70–75
28. Sakakibara R, Tateno F, Kishi M, Tsuyusaki Y, Terada H, Inaoka T (2014) MIBG myocardial scintigraphy in pre-motor Parkinson's disease: a review. *Parkinsonism Relat Disord* 20:267–273
29. Cacciola A, Milardi D, Anastasi GP et al (2016) A Direct Cortico-Nigral Pathway as Revealed by Constrained Spherical Deconvolution Tractography in Humans. *Front Hum Neurosci* 10:374
30. Sesack SR, Deutch AY, Roth RH, Bunney BS (1989) Topographical organization of the efferent projections of the medial prefrontal cortex in the rat: an anterograde tract-tracing study with Phaseolus vulgaris leucoagglutinin. *J Comp Neurol* 290:213–242
31. Kunzle H (1978) An autoradiographic analysis of the efferent connections from premotor and adjacent prefrontal regions (areas 6 and 9) in macaca fascicularis. *Brain Behav Evol* 15:185–234
32. Kwon HG, Jang SH (2014) Differences in neural connectivity between the substantia nigra and ventral tegmental area in the human brain. *Front Hum Neurosci* 8:41
33. Peran P, Cherubini A, Assogna F et al (2010) Magnetic resonance imaging markers of Parkinson's disease nigrostriatal signature. *Brain* 133:3423–3433
34. Hattori T, Orimo S, Aoki S et al (2012) Cognitive status correlates with white matter alteration in Parkinson's disease. *Hum Brain Mapp* 33:727–739
35. Song SK, Lee JE, Park HJ, Sohn YH, Lee JD, Lee PH (2011) The pattern of cortical atrophy in patients with Parkinson's disease according to cognitive status. *Mov Disord* 26:289–296
36. Nishio Y, Hirayama K, Takeda A et al (2010) Corticolimbic gray matter loss in Parkinson's disease without dementia. *Eur J Neurol* 17:1090–1097
37. Braak H, Del Tredici K, Bratzke H, Hamm-Clement J, Sandmann-Keil D, Rub U (2002) Staging of the intracerebral inclusion body pathology associated with idiopathic Parkinson's disease (preclinical and clinical stages). *J Neurol* 249:III/1–III/5
38. Chan LL, Rumpel H, Yap K et al (2007) Case control study of diffusion tensor imaging in Parkinson's disease. *J Neurol Neurosurg Psychiatry* 78:1383–1386
39. Benjamini Y, Hochberg Y (1995) Controlling the false discovery rate: a practical and powerful approach to multiple testing. *J R Stat Soc Ser B* 57:289–300
40. Woo CW, Krishnan A, Wager D (2014) Cluster-extent based thresholding in fMRI analyses: Pitfalls and recommendations. *Neuroimage* 91:412–419